High-Resolution ^{19}F MAS NMR Spectroscopy of Fluorocarbon Films from Pulsed PECVD of Hexafluoropropylene Oxide

Kenneth K. S. Lau and Karen K. Gleason*

Department of Chemical Engineering, Massachusetts Institute of Technology, Cambridge, Massachusetts 02139

Received: February 22, 1998; In Final Form: April 24, 1998

Magic angle sample spinning with speeds of up to 25 kHz has been applied to obtain high-resolution solid-state ^{19}F NMR spectra of fluorocarbon films deposited by pulsed plasma-enhanced chemical vapor deposition (PECVD) from hexafluoropropylene oxide. Compared to XPS, the common characterization method for fluorocarbon thin-film analysis, ^{19}F NMR is demonstrated to provide greater structural information which is important in unraveling the complexity of plasma films. Seven fluorocarbon resonances—three CF_3 sequences, three CF_2 sequences, and a CF resonance—were distinguished, based on differences in next nearest-neighbor bonding environment. Total CF_x ($x = 1-3$) fractions, as quantified by NMR, agreed with independent XPS results. Line width variation of the assigned resonances resulted from isotropic shift dispersion, arising from connectivity permutation statistics and from the relative mobility of fluorocarbon moieties, which can be hindered by cross-links or branch junctions. With lower pulsed plasma deposition duty cycles, resulting films contained more linear CF_2 chains. Cross-linking, branching, and irregular chain terminations, arising from plasma ion bombardment and excessive gas-phase fragmentation during film growth, are reduced. The thermal decomposition mechanism shifted from a loss of CF_3 end groups to a loss of linear chain fragments as a result of changes in film structure with longer deposition pulse off-time. There is evidence to indicate thermal desorption of oligomers or radical-enhanced depolymerization for films deposited at lower duty cycles.

Introduction

Fluorocarbon thin films grown by plasma-enhanced chemical vapor deposition (PECVD) have been extensively studied by X-ray photoelectron spectroscopy (XPS).[1,2] In particular, carbon 1s XPS provides sufficient sensitivity in electronic shifts to enable carbon nuclei to be differentiated based on the number of directly bonded fluorines, as binding energy shifts by ~+2 eV for each additional fluorine. Spectral regression then allows the relative amount of each CF_x ($x = 0$, 1, 2, or 3) fraction to be determined, thereby providing information on film composition.

In this paper, we demonstrate the greater efficacy of solid-state ^{19}F nuclear magnetic resonance (NMR) spectroscopy for providing more detailed structural information on PECVD fluorocarbon films than is derivable from XPS. High sensitivity of the fluorine nucleus to its local bonding and electronic environment translates to a large spectral chemical shift range (>200 ppm). Thus, ^{19}F NMR is capable of resolving fluorocarbon species based on differences in neighboring connectivities, making it possible to identify different fluorocarbon sequences with lengths of three carbons or more. Such detailed information is especially profitable in understanding the complexity of the plasma film network. The 100% isotopic abundance and high magnetogyric ratio of ^{19}F also makes it an excellent candidate for NMR observation even with relatively small sample sizes as is the case in thin-film analysis. Recent advances in magic angle spinning (MAS) NMR probes, achieving sample spinning speeds of up to 25 kHz, have also allowed sufficient averaging of intrinsic spectral broadening from strong dipolar interaction and chemical shift anisotropy that high-resolution ^{19}F NMR studies in the solid state are becoming routine.[3−6]

Specifically, our motivation for using high-resolution ^{19}F NMR in this study is to probe more deeply into the structural network of fluorocarbon films deposited by pulsed PECVD using hexafluoropropylene oxide (HFPO) as the reactant gas. Unlike conventional PECVD, pulsed PECVD applies radio-frequency (rf) pulses to excite the source gas to periodically generate the plasma for film deposition. Pulsing the plasma is believed to allow a higher selectivity of desirable activated neutrals over undesirable ions and electrons in film deposition reactions,[7] offering greater control over the molecular design and composition of fluorocarbon thin films to meet the needs of their potential applications, such as biopassivation coatings for clinical implants and dielectric layers in microelectronic devices. By a suitable choice of source gas, fluorocarbon films from pulsed PECVD having either a high CF_2 fraction[8−10] or CF_3 fraction[11] have been reported. In contrast, films from continuous PECVD contain nearly equal amounts of CF_3, CF_2, CF, and quaternary carbon moieties regardless of the source gas fed.[2,12]

Ultimately, our goal is to attain a good understanding of the structure−property−processing relationship of fluorocarbon films to the pulsed PECVD process. This will aid in materials development to realize intended applications, and high-resolution ^{19}F NMR is a valuable tool which will facilitate immensely to that end.

Experimental Section

Fluorocarbon films were grown on 100 mm diameter silicon substrates by pulsed PECVD of hexafluoropropylene oxide (C_3F_6O) (PCR Incorporated) for pulse cycles of 10/50, 10/200, and 10/400 ms on-/off-times. Deposition was done in a parallel plate, capacitively coupled reactor system using 13.56 MHz

* Corresponding author. E-mail kkgleasn@mit.edu.

S1089-5647(98)01240-1 CCC: $15.00
Published on Web 07/10/1998

pulsed rf excitation. Details of reactor configuration and deposition conditions are given elsewhere.[13,14] Films from deposition at each pulse condition were scraped off the substrate for subsequent analyses.

All NMR experiments were performed on a home-built spectrometer tuned to 254.0 MHz for ^{19}F detection. A Chemagnetics 3.2 mm double-resonance solids probe capable of a maximum sample spinning speed of 25 kHz was used to perform high-resolution MAS. Film samples for spinning were packed into zirconia rotors having an internal volume of 11 mm^3, representing sample weights of 15−20 mg. A Chemagnetics MAS speed controller maintained rotor speed to within ±3 Hz of the set point. The spinning module housing, rotor end caps, spacers, and drive tips were made of Vespel or Torlon to minimize ^{19}F background signal. Spectra were acquired with a 90° pulse duration of 1.25 μs and a spectral window of observation set at ±250 kHz. Acquisition delay of 10 s was determined to be sufficient for obtaining quantitative spectra. All spectral chemical shifts were referenced to $CFCl_3$.

The total suppression of spinning sidebands (TOSS) sequence,[15] $\{\pi/2-\tau_1-\pi-\tau_2-\pi-\tau_3-\pi-\tau_4-\pi-\tau_5-$acquisition; where $\tau_1 = 0.1226\tau_r$, $\tau_2 = 0.0773\tau_r$, $\tau_3 = 0.2236\tau_r$, $\tau_4 = 1.0433\tau_r$, $\tau_5 = 0.7741\tau_r$, and τ_r is one rotor period$\}$, was applied at a spinning speed of 23 kHz to obtain spectra free of residual sidebands and to facilitate isotropic peak identification. Direct excitation at 25 kHz MAS produced spectra for quantitation, but the presence of some residual fluorine background from outside the spinner assembly required a DEPTH technique,[5] $\{\pi/2-\pi-\pi-$acquisition; 16-step phase cycle$\}$, to effectively suppress any unwanted signal and to remove systematic errors. Spectral regression assumed full Lorentzian line shapes. Quantitation results were compared to corresponding XPS data and were studied in relation to the effect changes in deposition pulse condition have on film structure.

Further analysis was made on film thermal stability for films from the 10/50 and 10/400 pulse cycles. NMR spectra were acquired using a 20 kHz MAS spin echo sequence, $\{(\pi/2)_x-\tau-(\pi)_y-\tau-$acquisition$\}$, with an echo delay τ of 50 μs and an acquisition delay of 120 s. Annealing prior to NMR detection was performed in an oven (NAPCO) with a continuous nitrogen purge, and the amount of weight loss was determined through weighing using a Mettler balance. To allow an unbiased comparison between spectra before and after annealing, a known weight of sodium fluoride (NaF) was also placed together with each weighed film sample inside the rotor during packing. The integrated NaF signal allowed normalization of each spectrum to an equivalent ^{19}F intensity per gram of NaF. The NaF standard accounted for differences resulting from variations in probe tuning and matching on different samples. Further spectral scaling was needed to account for weight of the film sample packed into each rotor.

Results and Discussion

Isotropic Peak Assignment. Figure 1 shows the ^{19}F TOSS spectra acquired at 23 kHz MAS. Because of strong $^{19}F-^{19}F$ dipolar couplings and large anisotropic chemical shielding extending over 25 kHz, residual spinning sidebands can still be observed in direct excitation or spin echo spectra (see following sections). Some of these sidebands overlap with isotropic resonances and interfere with peak identification so TOSS was applied to effectively remove the presence of these sidebands. Consequently, seven main resonances can be identified, and assignments are given in Table 1. The assignments were made by appropriately matching their chemical shift

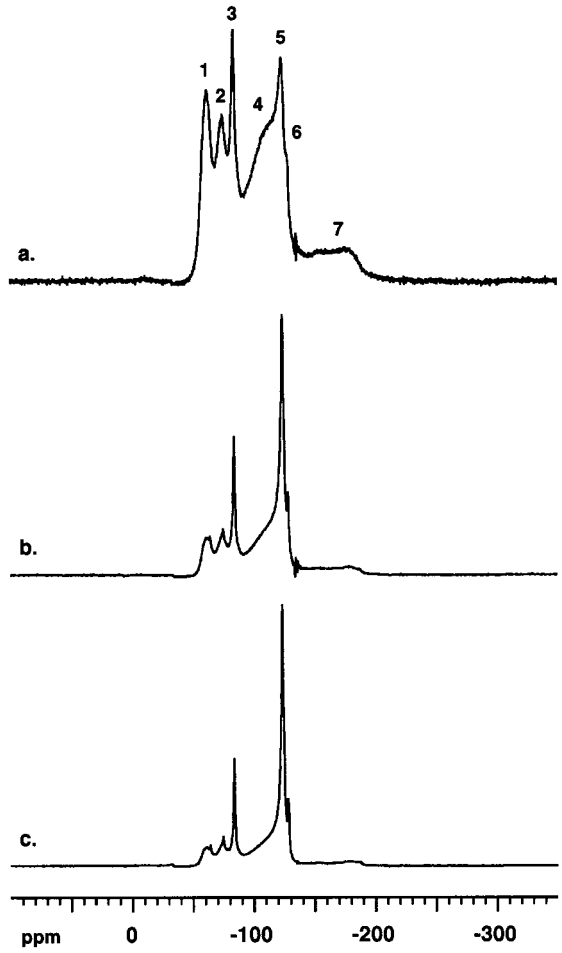

Figure 1. The 23 kHz ^{19}F TOSS spectra of **(**a**)** 10/50, **(**b**)** 10/200, and **(**c**)** 10/400 pulsed PECVD films of HFPO; 64 transients, 8192 points. The seven main resonance assignments are summarized in Table 1.

TABLE 1: Spectral Assignments of Fluorocarbon Resonances in Pulsed PECVD Films of HFPO

peak	CF_x sequence[a]	peak	CF_x sequence[a]
1	CF_3*C	5	CF_2CF_2*CF_2
2	CF_3*CF	6	CF_2CF_2*CF_3
3	CF_3*CF_2	7	CF*
4	$CF_x CF_2$*CF_x[b]		

[a] Asterisk denotes the fluorine nucleus of NMR detection. [b] Subscript *x* denotes the variety of fluorocarbon groups possible and can vary from 0 to 3 depending on admissibility, i.e., excludes sequences of peaks 5 and 6 and sequence of gaseous $CF_3CF_2CF_3$.

range with published chemical shifts for various fluorocarbon structures as summarized in Table 2.[3,4,16−20]

Peaks 1, 2, and 3 are attributed to CF_3 moieties having different next-nearest neighbors, with each CF_3 peak being shifted upfield from the previous as a result of an additional fluorine on its α-carbon. (The convention adopted herein will refer to α- and β-positions relative to the *carbon* having the fluorine nuclei of direct NMR observation, e.g., a CF_2CF_2*CF_3 sequence will have two α-carbons and five β-fluorines with respect to the two directly detected fluorines on the carbon of reference.) Lack of shift sensitivity to differences in the number of fluorines on the β-carbon and beyond precludes further finer resolution, although with spectra of the 10/200 and 10/400 films, some sharper resonances within peaks 1 and 2 suggest the assigned peaks may consist of more detailed structures than is offered by Table 1. CF_2 moieties are assigned to peaks 4, 5,

TABLE 2: ^{19}F Isotropic Chemical Shifts for Representative Fluorocarbon Groups

CF_x[a]		$\sigma_{iso,F}$[b]	ref
CF_3	$(CF_3{*})_3C-$	−62, −64	16, 17
	$(CF_3{*})_2C=$	−61	18
	$CF_3{*}C=$	−50, −54	3
	$(CF_3{*})_2CF-$	−73, −74, −76	19
	$CF_3{*}CF-$	−71, −72, −73	4, 20
	$CF_3{*}CF=$	−71, −72	18
	$CF_3{*}CF_2CF_2-$	−82, −83, −84	3, 16
	$CF_3{*}CF_2CF-$	−80, −82	18
CF_2	$-CF_2CF=CF_2{*}$	−93, −109	16
	$-CFCF_2{*}CF_3$	−114	18
	$-CFCF_2{*}CF_2-$	−110, −111	18, 20
	$-CF_2CF_2{*}CF_2-$	−123, −124	3, 4
	$-CF_2CF_2{*}CF_3$	−128, −129	3, 18
CF	$-CF{*}(CF_3)_2$	−175, −187	19
	$-CF_2CF{*}(CF_3)CF_2-$	−182	20
	$-CF_2CF{*}=CF_2$	−191	16

[a] Asterisk denotes the fluorine nucleus of NMR detection. [b] Chemical shifts are referenced in ppm to $CFCl_3$.

and 6, with the most downfield peak (peak 4) being significantly broader than the other two. Chemical shifts of peaks 5 and 6 agree well with literature values for linear CF_2 chain sequences, positioned internally and with one α-CF_3 termination, respectively. It is reasonable to assign peak 4 to CF_2 moieties having α-carbons that are less fluorinated compared to those in peaks 5 and 6. This results in a large number of permutations of α- and β-carbon connectivities which in turn leads to substantial isotropic shift dispersion and broadening of the peak. Such heterogeneous broadening unfortunately cannot be narrowed by MAS at any speed.[21] For the same reason, peak 7 can only be identified as the CF resonance for lack of resolution in separating out CF moieties based on different neighbor environments. As will be seen later, there is strong evidence to suggest part of the line broadening is also attributable to a lack of motional narrowing in these fluorocarbon moieties.

CF_x Quantitation. To obtain quantitative information on each assigned resonance, regression of 25 kHz ^{19}F MAS direct excitation spectra was required. Two factors prompted this need. First, from the TOSS spectra (Figure 1), it is clear the seven assigned resonances are not completely separated from each other. This overlap precludes quantitation of the various species through direct spectral integration. Second, the areas of the spinning sidebands, some of which overlap with the CF resonance, have to be accounted for. Thus, regression was performed by fitting the actual data to a sum of Lorentzian line shapes through minimizing the χ^2 error. At sufficiently high MAS speeds, line shapes of isotropic peaks and spinning sidebands are anticipated to be Lorentzian in nature.[22] Figure 2 demonstrates the goodness of fit of the regressed spectra.

Although Table 1 only identifies seven distinct fluorocarbon sequences, a total of 22 Lorentzian functions were required to represent isotropic peaks. Further Lorentzians were used to delineate spinning sidebands. These were constrained at integral multiples of ±25 kHz from their corresponding isotropic peak positions. Figure 3 gives a partial breakdown of the regression within the isotropic region for the representative case of the 10/50 film, showing summed contributions to each assigned resonance. For clarity, spinning sideband contributions are not shown. From Figure 3, regression results in significantly broader line widths for peaks 4 and 7 compared to the others. This is in agreement with experimental and statistical observations discussed below and thus lends credence to the validity of the regression analysis.

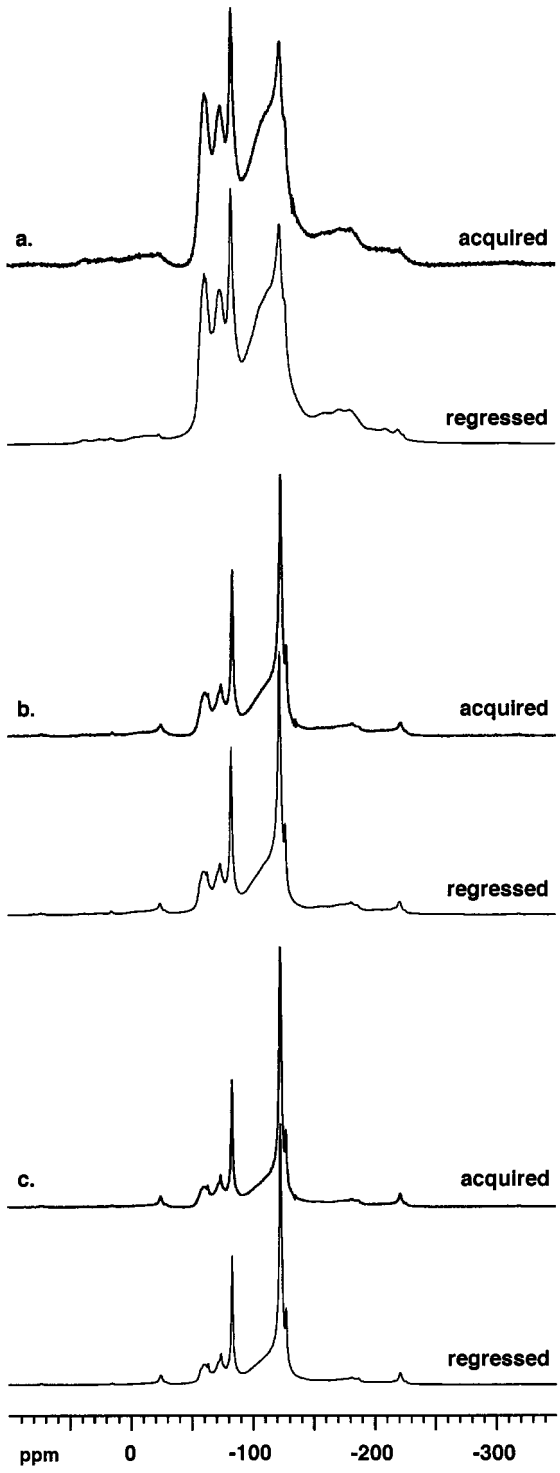

Figure 2. The 25 kHz ^{19}F MAS spectra of **(a)** 10/50, **(b)** 10/200, and **(c)** 10/400 pulsed PECVD films of HFPO; direct excitation with DEPTH background suppression; experimental and regressed; 64 transients, 8192 points. Spectral regression was performed by fitting a sum of Lorentzians to the data and minimizing the χ^2 error. Twenty-two isotropic peaks and additional peaks to account for residual spinning sidebands, spaced from the isotropic peaks at integral multiples of the rotational frequency, were required to achieve a good fit.

Line broadening, under conditions of high-resolution MAS, can be attributed in part to the relative mobility of fluorocarbon fragments within the assigned resonances. Evidence comes directly from additional 25 kHz ^{19}F MAS spin echo experiments done on the 10/50 film for prolonged $\tau = n\tau_r$ echo delays (τ_r is one rotor period), as shown in Figure 4. With an echo delay

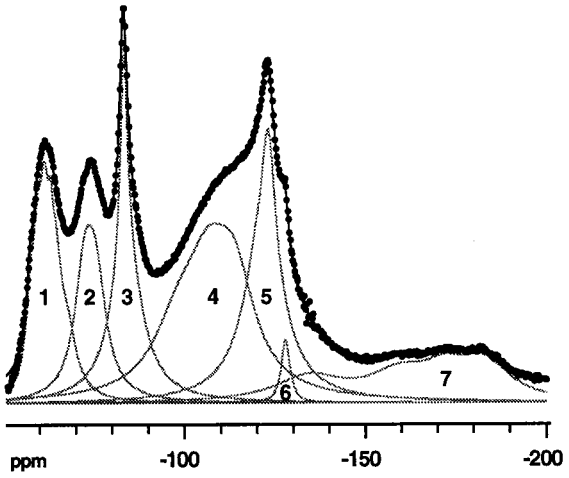

Figure 3. Breakdown of regression on direct excitation spectrum of 10/50 pulsed PECVD film of HFPO into the seven assigned resonances. Solid circles, black line, and gray lines represent experimental data, total regressed fit, and the individual components regressed fits, respectively. The individual fits were obtained by summing Lorentzian contributions within that particular resonance. Significantly larger predicted line widths for peaks 4 and 7 were attributed to both their larger number of extended bond connectivity permutations and their lower mobility.

of 1 ms (Figure 4a), intensities from the CF_xCF_2*CF_x and CF* resonances (peaks 4 and 7) are no longer discernible. Only signals from those of more mobile species of linear CF_2 chain fragments and especially CF_3 chain terminations are observed. This spectral editing takes advantage of the significantly faster T_2 relaxation rates of CF_xCF_2*CF_x and CF* species as a consequence of their lower mobility, since fluorocarbon groups either with more cross-linking neighbors or are cross-linking moieties themselves naturally suffer greater steric hindrance in their internal movements. As line width is inversely related to T_2, this agrees with the predicted line width behavior from regression.

Another source of line broadening stems from the numerous permutations of bond connectivities in a plasma film matrix. From a purely statistical standpoint, the number of permissible sequences within peaks 4 and 7 based on differences up to the β-carbon level would be extremely large (>100). Consequently, because chemical shift sensitivity to differences in neighboring attachments decreases with increasing bond distance from the observed fluorine nucleus, these permutations become too closely spaced to be resolved into individual lines but instead overlap to yield a broad composite resonance. Peaks 1, 2, and 3, on the other hand, are predicted to have narrower line widths. Once again, if the number of β-carbon permutations is considered, as given in Table 3, the smaller number of sequences implies less severe isotropic shift dispersion. Furthermore, the decreasing trend in going from peak 1 to 3 matches the decrease in line broadening as indicated by the regression results. A similar agreement is observed between the predicted line width and the number of permutations for peaks 5 and 6 (Table 3). Experimental support for the existence of finer lines within the assigned resonances can be seen from spin echo spectra at longer echo delays of 2 and 3 ms (Figure 4, b and c). Finer structures within the CF_3 resonances become more noticeable and are similar to features in direct excitation spectra of the 10/200 and 10/400 films (Figure 2, b and c).

As a confirmation of the regression methodology, a comparison of quantitation results from NMR with corresponding XPS data is worthwhile. Regression of direct excitation spectra

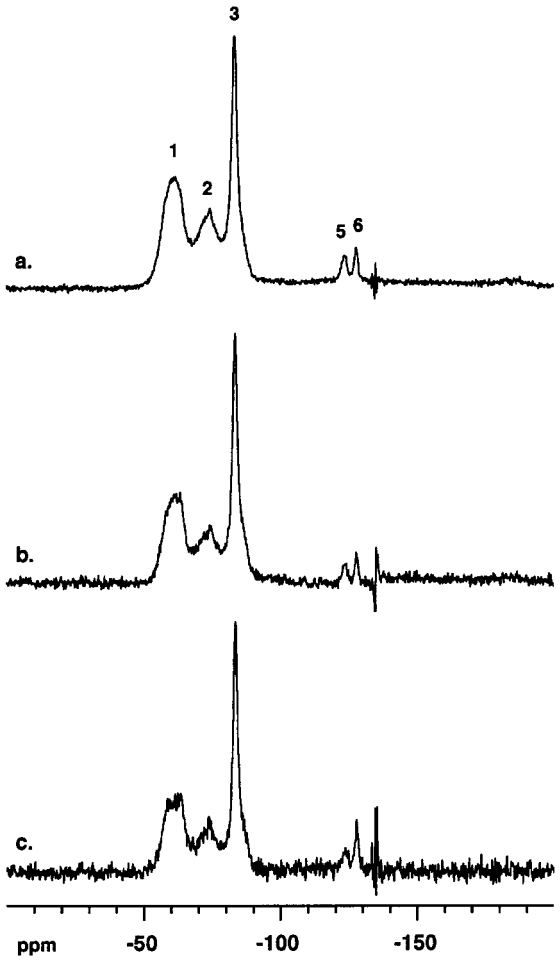

Figure 4. The 25 kHz ^{19}F MAS spin echo spectra of 10/50 pulsed PECVD film of HFPO using echo delays of **(**a**)** 1, **(**b**)** 2, and **(**c**)** 3 ms; 256, 1024, and 2048 transients respectively; 4096 points; sweep width of ±125 kHz was used for this series of spectra. Long echo delays enabled efficient T_2 filtration, selecting the more mobile species of chain ends and linear chain fragments. Moieties involved in cross-linking and branching or have such next-nearest neighbors (peaks 4 and 7) naturally suffer movement constraints and were selectively lost as a result of shorter T_2.

TABLE 3: Connectivity Permutation Statistics of Fluorocarbon Resonances in Pulsed PECVD Films of HFPO

peak	CF_x sequence[a]	N[c]
1	$\{CF_3{*}C\}(CF_x)_3$[b]	19
2	$\{CF_3{*}CF\}(CF_x)_2$	9
3	$\{CF_3{*}CF_2\}CF_x$	3
4	$CF_x\{CF_xCF_2{*}CF_x\}CF_x$	>100
5	$CF_x\{CF_2CF_2{*}CF_2\}CF_x$	12
6	$CF_x\{CF_2CF_2{*}CF_3\}$	3
7	$\{CF{*}\}(CF_x)_3(CF_x)_3$	>100

[a] Asterisk denotes the fluorine nucleus of NMR detection. [b] Subscript x denotes the variety of fluorocarbon groups possible and can vary from 0 to 3 depending on admissibility. Excludes any gaseous small fluorocarbon molecules. [c] N = number of bond permutations up to the β-carbon environment. Unsaturation, which will only add to the statistics without modifying the general trend, is ignored.

allowed the intensities of the seven assigned resonances to be separately calculated. Subsequently, to determine the relative fraction of each CF_x species, intensities belonging to the same observed fluorocarbon moiety were grouped, i.e., CF_3, 1 + 2 + 3; CF_2, 4 + 5 + 6; and CF, 7. These values were then compared with corresponding XPS data from an extensive compositional study by Limb et al. on pulsed PECVD films of

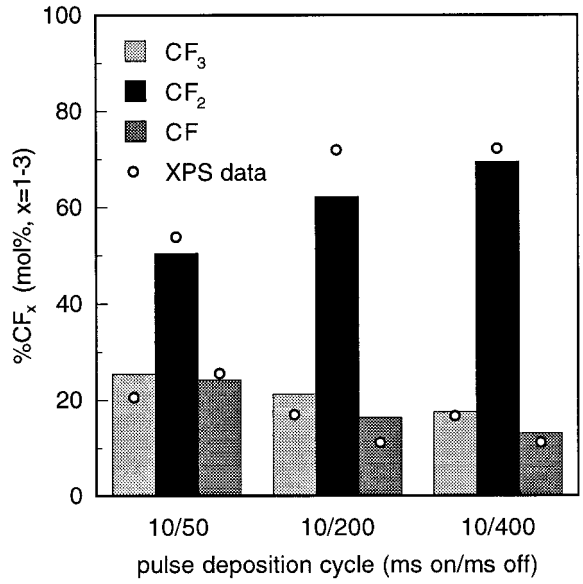

Figure 5. Comparison of NMR and XPS data on % CF_x ($x = 1-3$) of 10/50, 10/200, and 10/400 pulsed PECVD films of HFPO. Bars are from NMR data of this work while open circles represent XPS data from ref 10. These percentages exclude quaternary carbon species. Agreement between NMR and XPS results validated the regression methodology and in turn demonstrated compositional homogeneity throughout the entire film.

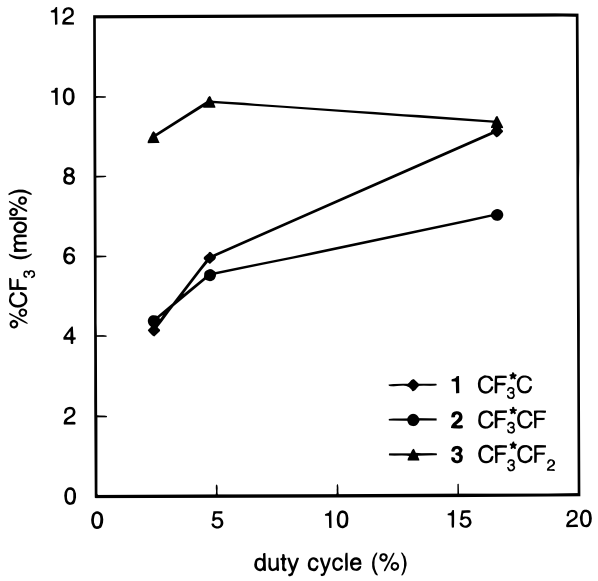

Figure 6. Variation in the amount of assigned CF_3 fragments with pulse deposition duty cycle. These percentages exclude quaternary carbon species. Lower duty cycles decreased the amount of irregular chain termination.

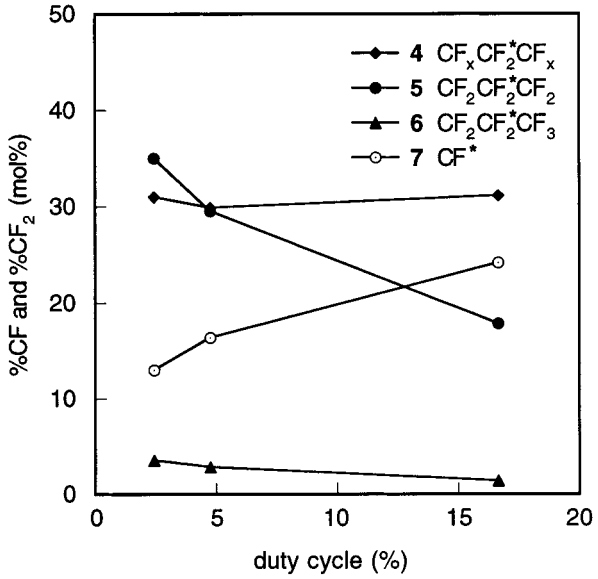

Figure 7. Variation in the amount of assigned CF_2 and CF fragments with pulse deposition duty cycle. These percentages exclude quaternary carbon species. Lower duty cycles decreased the amount of cross-linking and branching junctions and simultaneously increased linear chain propagation.

HFPO.[10] Figure 5 plots the CF, CF_2, and CF_3 fractions present in the 10/50, 10/200, and 10/400 films as derived from NMR and XPS. Remarkably good agreement between these vastly different characterization methods offers two implications. The NMR regressions are reasonably accurate in their representations of actual spectra, and peak assignments are unambiguously verified. In turn, even though XPS is surface sensitive while NMR analyzes the bulk material, results point to compositional homogeneity throughout the entire film structure. Slight deviations for the 10/200 film are probably due to greater detection sensitivity of NMR to smaller compositional changes compared to XPS.

Film Structure vs Deposition Pulse Condition. From Figure 5, it is already evident that pulsing an HFPO plasma during PECVD has a profound effect on resulting film composition. For increasing pulse off-times at constant on-times, the proportion of CF_2 moieties increases dramatically relative to CF_3 and CF fractions. Unfortunately, ^{19}F NMR does not provide direct information on quaternary carbons, but XPS has shown that there are also less of these moieties with longer pulse off-times.[10] To look closer at how individual fluorocarbon fragments are affected by deposition pulse conditions, Figures 6 and 7 trace out the variation of the seven assigned resonances as a function of duty cycle (defined as the ratio of on-time to total cycle period). These figures, as in Figure 5, show fluorocarbon percentages based on observed CF_x species ($x = 1-3$), i.e., excluding unobservable quaternary carbons.

Most noticeably, there is a tradeoff between the amount of CF* and CF_2CF_2*CF_2 fragments that are present within these fluorocarbon films, with the latter becoming more prevalent at lower duty cycles (longer off-times). This corroborates with the hypothesis that, during the period when the plasma is extinguished, the longer-lived difluorocarbene radicals present inside the plasma have more time to polymerize linearly into chains much like poly(tetrafluoroethylene) (PTFE).[14] These radicals have been shown to form during thermal decomposition of HFPO,[23] and the plasma can be expected to generate an appreciable amount of such radicals via electronic excitation.

Lower duty cycles also reduce the extent of undesirable gas-phase fragmentation, since ions and electrons responsible for such processes are quenched more quickly than activated neutrals within the pulse off-time. Bombardment of these energetic species at the film surface, which may lead to structural rearrangement, cross-linking, etching, or defluorination of the film, is diminished as well. These interpretations are supported by the reduction in the number of CF*, CF_3*C, and CF_3*CF fragments, fragments which are not involved in linear chain propagation. Interestingly, however, CF_xCF_2*CF_x is one fluorocarbon fraction that does not seem to vary with changes in film deposition duty cycle, even though its immediate neighbors are either nonpropagating or cross-linking fluorocarbon units. With

pulse on-time being one important process variable that remained constant during deposition, it is reasonable to surmise that the formation of these moieties is probably confined to within the duration of plasma discharge of each pulse cycle. These observations offer some idea of how various pulsing variables have a bearing on what type of building blocks are ultimately incorporated into the film.

Insight can also be drawn from the apparent anomaly between the fractions of CF_3*CF_2 and CF_2CF_2*CF_3 groups (peaks 3 and 6). The former remains roughly constant at just below 10 mol % while the latter is far lower and increases only slightly with increasing pulse off-time. This lack of agreement can be explained by recognizing that peak 3 accounts for CF_3*CF_2 groups with other β-CF_x ($x < 2$) groups in addition to β-CF_2 groups. Table 2 clearly evidences chemical shifts of CF_3*CF_2-CF_2 and CF_3*CF_2CF sequences being in proximity with each other (<5 ppm), both of which are within the range of peak 3. In contrast, as Table 2 also attests, peak 6 is assigned solely to CF_2CF_2*CF_3 groups because all other CF_2 groups having one α-CF_3 chain termination and another α-CF_x ($x < 2$) neighbor reside within the shift range of peak 4, CF_xCF_2*CF_x species. Thus, the discrepancy points to a fair amount of premature chain termination at the β-carbon away from branch or cross-link junctions. The reason for this is not entirely clear, but there may be a favorable reaction pathway involving plausibly the addition of an activated three-carbon HFPO molecule to the network, forming a two-carbon branch and simultaneously eliminating a volatile carbonyl fluoride, COF_2. The lack of oxygen incorporation within the film, as indicated by XPS,[14] and the presence of COF_2 in some oxygen-containing fluorocarbon plasmas, as shown through gas-phase diagnostics,[24,25] seem to support such a hypothesis. Alternatively, the discrepancy may simply be a result of the statistical nature of the film network, with the CF_3*CF_2 sequence having a larger number of extended bond connectivity permutations than is possible with the CF_2CF_2*CF_3 sequence.

Thermal Decomposition Study. In an attempt to investigate the thermal stability of pulsed HFPO films, annealing of films from the 10/50 and 10/400 pulse conditions was performed, and changes in structure were traced through differences in spectral features between the pristine and annealed samples. These results are shown in Figures 8 and 9, respectively, for 1 h nitrogen anneals at 150 °C. Previous thermogravimetric analysis (TGA) on these films indicated weight loss commencing in the range 100−150 °C, with an average loss rate on the order of 10^{-4} mg/(cm^2 s).[26] Because TGA only measures weight loss, NMR is conveniently extended here to provide greater insight into the sources of such film loss.

Comparing films from the two duty cycles, difference spectra (Figures 8c and 9c) clearly indicate different degradation mechanisms. For the 10/50 film, the more unstable bonding environments are CF_3 terminations. Because the film has comparatively more cross-links and branches, it is appropriate to understand how thermal degradation can be significantly influenced by the presence of these units. Tortelli et al. have made an insightful contribution to understanding the thermal decomposition pathways of branched perfluoroalkanes.[19] Carbon−carbon bonds were found to be weaker with more perfluoroalkyl substitutions, and bond scissions occurred at the most substituted sites. Also, loss of CF_3 was favored when the radical formed could be readily stabilized. Directing these conclusions to the 10/50 film, loss of CF_3 from CF_3*C or CF_3*CF junctions will naturally yield radicals that can be easily stabilized by being positioned at highly substituted carbon sites.

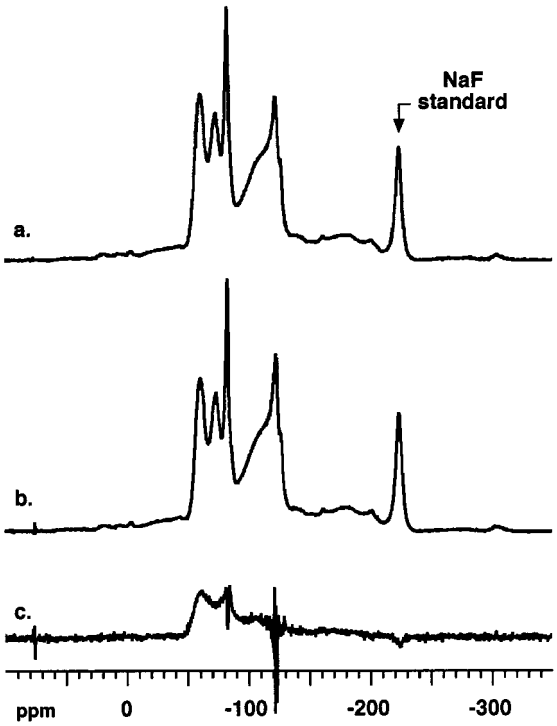

Figure 8. The 20 kHz ^{19}F MAS spin echo spectra of 10/50 pulsed PECVD film of HFPO for **(**a**)** pristine and **(**b**)** annealed samples, using an echo delay of 50 μs, while **(**c**)** is the resulting difference spectrum; 128 transients, 8192 points. Spectra a and b have been scaled appropriately to represent the actual spectral change upon annealing at 150 °C for 1 h in a nitrogen ambient. Peak arising from internal NaF standard used in the scaling is marked. Spectrum c has been expanded for clarity. In this relatively more cross-linked film, termination groups were preferentially lost upon annealing.

Loss of CF_3 from CF_3*CF_2 groups, on the other hand, is more likely due to loss of *entire* CF_3*CF_2 fragments from CF_3*CF_2 sequences with a branch or cross-link β-carbon. Evidence can be derived from Figure 8c, which shows corresponding loss from the CF_xCF_2*CF_x region but practically no loss from the CF_2-CF_2*CF_3 peak. Furthermore, Tortelli et al. observed that a perfluoroethyl branch, presumably due to higher steric stress, was considerably weaker than a trifluoromethyl branch.[19]

For the 10/400 film, film loss is concentrated in the linear fluorocarbon chain regions, with elimination of CF_2CF_2*CF_2 and CF_2CF_2*CF_3 fragments. This seems to suggest that the degradation mechanism may be one of linear chain depropagation, characteristic of chain unzipping in PTFE when it thermally decomposes in a vacuum to yield its monomer.[27] To further probe this interesting development for the 10/400 film, separate annealings of pristine samples were done at 200 and 250 °C, and corresponding spectra were acquired. From the difference spectrum of each annealed sample against the pristine film, intensity loss in the CF_2CF_2*CF_2 and CF_2CF_2*CF_3 resonances was followed as a function of temperature and plotted as an Arrhenius relationship, as shown in Figure 10. The activation energy for the loss of both these groups was calculated to be 3.4 kcal/mol. This result is surprisingly low compared to the activation energy for a carbon−carbon bond dissociation, which for fluorocarbons is reported to be 81.5 kcal/mol.[28]

One possible interpretation is the presence of short-chain perfluoroalkane oligomers of PTFE within the 10/400 film. If the ratio of the intensities of CF_2CF_2*CF_2 to CF_2CF_2*CF_3 fragments (peak 5/peak 6) were computed for the as-deposited film, a value of around 10 is obtained. This means that, for

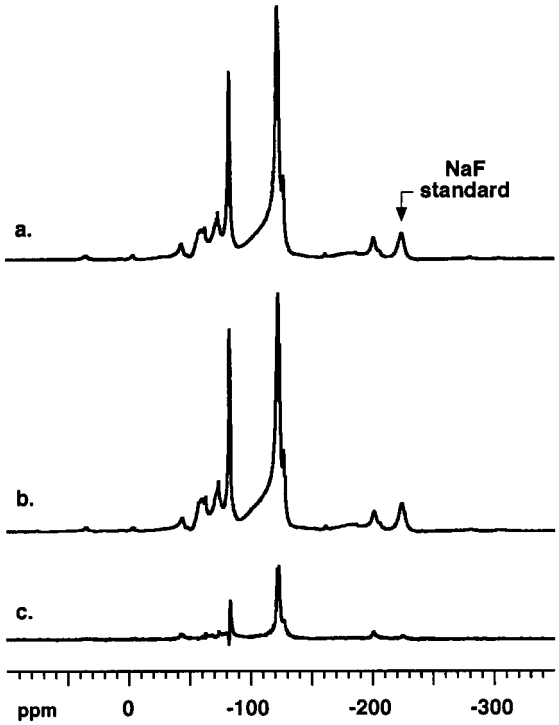

Figure 9. The 20 kHz ^{19}F MAS spin echo spectra of 10/400 pulsed PECVD film of HFPO for **(**a**)** pristine and **(**b**)** annealed samples, using an echo delay of 50 μs, while **(**c**)** is the resulting difference spectrum; 128 transients, 8192 points. Spectra a and b have been scaled appropriately to represent the actual spectral change upon annealing at 150 °C for 1 h in a nitrogen ambient. Peak arising from internal NaF standard used in the scaling is marked. Linear chain type fragments were preferentially lost for this less cross-linked film.

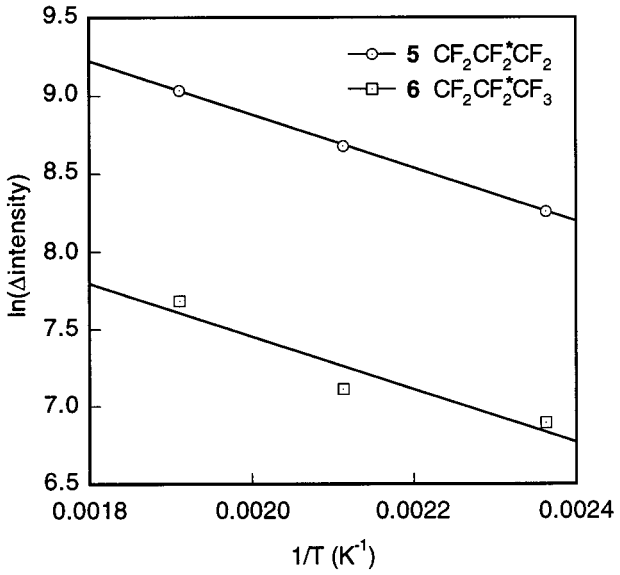

Figure 10. Arrhenius plot of spectral intensity change upon thermal annealing of 10/400 pulsed PECVD film of HFPO at temperatures of 150, 200, and 250 °C. Since annealing time is constant for each temperature, the rate of intensity loss is proportional to the absolute intensity loss. Activation energy derived from both lines was 3.4 kcal/mol and possibly reflected physical desorption of oligomeric chains or depolymerization facilitated by radicals present in the pristine film.

every two CF_3 chain ends, there would be 22 internal CF_2 units. Being aware this ratio is only an average value, it nonetheless represents a $C_{24}F_{50}$ chain. Comparing this hypothetical chain to one of similar size, perfluoroeicosane ($C_{20}F_{42}$), the latter has a melting point of 165 °C, which is close to the temperature at which decomposition is initially observed for the 10/400 film. There is indication that gas-phase addition reactions cannot be ignored during pulsed PECVD of HFPO,[14] and with a longer pulse off-time, there is a greater likelihood for these addition species to adsorb and become trapped within the growing film. Gas-phase polymerization has been observed in continuous plasmas of fluorocarbon gases, and by electron attachment mass spectrometry (EAMS) products containing up to 10 carbons were identified, this being constrained only by the mass detection limit of the instrument.[29] Oligomer formation can also occur on the film surface itself. Plasma degradation of the film during deposition may cause cleavage of chains growing on the film surface, resulting in low molecular weight chains which become trapped as the film grows.[30] Recent thermal cycling studies of amorphous carbon films containing fluorine and hydrogen have proposed the ejection of occluded volatiles as a possible source of film thermal instability.[31] Furthermore, thermal desorption spectroscopy (TDS) of fluorocarbon films deposited from a continuous C_2F_4/Ar plasma found degassing or decomposition starting at temperatures of around 120−140 °C and products included not only trapped C_2F_4 precursor but also a wide range of low molecular weight fluorocarbon molecules.[32]

An alternative interpretation to the low activation energy that may be equally probable is the ease of chain depolymerization when a radical or dangling bond site is already present along the linear chain in the pristine film. Indeed, irradiation of PTFE with γ-rays is known to reduce polymer melting point[33] and accelerate thermal decomposition by enhancing radical initiation.[34] Thus, the presence of existing radicals in the 10/400 film will greatly facilitate the unzipping process to the extent where the energy barrier may become comparable to physical desorption. Plasma films are known to have an appreciable concentration of radical or dangling bonds, and although pulsing the plasma has the advantage of reducing these undesirable defects, as shown through electron spin resonance (ESR) spectroscopy,[13] there may still be a sufficient amount ($\sim 10^{18}$ spins/g) to induce chain depropagation. However, a counter-argument could be made against this hypothesis since such a decomposition mechanism is not observed in the 10/50 film, even though its dangling bond concentration is reportedly higher.[13] This can be rationalized by recognizing that the greater amount of cross-linking in the 10/50 film will most likely reduce the probability of internal fragmentation, since connectivities are efficiently intertwined and cross-links may have to be severed to free a chain fragment.

Having identified and discussed some of the major sources of thermal instability within plasma fluorocarbon films, the type of building blocks required for a stable film becomes apparent. Since losses from peaks 4 and 7 are negligible, greater thermal stability seems to be imparted through a more cross-linked network. This conclusion is also made by other work on plasma fluorocarbon films.[35] Though a cross-linked matrix necessitates a reduction in the amount of fluorine relative to carbon, it may still be possible to sustain an appreciable level of fluorination by interspersing CF_2 units between cross-links, i.e., dominated by moieties in peak 4, without compromising on film thermal stability.

Conclusion

High-resolution ^{19}F MAS NMR studies revealed significant differences between fluorocarbon films deposited by pulsed PECVD of HFPO at 10/50, 10/200, and 10/400 ms on-/off-times. Spectral separation to seven main resonances based on

chemical shift differences up to the α-carbon were achieved using spinning speeds of at least 20 kHz. The 23 kHz TOSS was applied to isolate isotropic peaks, and assignments were made by comparing with published shift values for comparable fluorocarbon moieties. Three CF_3 (CF_3*C, CF_3*CF, CF_3*CF_2), three CF_2 (CF_xCF_2*CF_x, CF_2CF_2*CF_2, CF_2CF_2*CF_3), and one CF peak were identified, each one being more upfield than the previous. Direct excitation at 25 kHz MAS produced spectra for quantitation of the seven environments. Results in terms of the fraction of each CF_x ($x = 1-3$) species agreed well with corresponding XPS data from an independent study. However, superior to XPS, NMR is able to distinguish within CF_x species differences in their neighboring attachments. This higher resolution beyond the immediate environment is attributed to the sensitivity of fluorine nuclei to their local electronic fields which NMR is able to detect. The broader line widths of the CF_xCF_2*CF_x and CF features were discussed in terms of isotropic shift dispersion due to their larger number of bonding permutations if sequences up to the β-carbon were considered and of their hindered mobility due to movement constraints from cross-linking and branching.

Revealing the finer details in bonding configurations enabled a more comprehensive understanding of the relationship between film structure and the pulsed plasma deposition process. This is especially valuable in the analysis of plasma deposited films where numerous reaction pathways can create a complex variety of bonding permutations. By increasing deposition pulse off-time, films showed more PTFE character, with an increase in the amount of linear chain propagation. This was attributed to less ion bombardment and more radical addition events. Further understanding of the relationship between the pulsed PECVD process and the thermal properties of these films was pursued in terms of structural changes upon thermal annealing. Thermal decomposition occurred via a CF_3 chain end detachment mechanism for films with more cross-linking and branching. Films with more linear fluorocarbon chain content showed loss of these chain units spectroscopically, and an Arrhenius study indicated desorption of short-chain oligomers or radical-enhanced chain depropagation as possible mechanisms.

Acknowledgment. We gratefully thank the NSF/SRC Engineering Research Center for Environmentally Benign Semiconductor Manufacturing for their support of this work.

References and Notes

(1) Yasuda, H. *Plasma Polymerization*; Academic Press: Orlando, FL, 1985.

(2) *Plasma Deposition, Treatment, and Etching of Polymers*; d'Agostino, R., Ed.; Academic Press: San Diego, 1990.

(3) Harris, R. K.; Jackson, P. *Chem. Rev.* **1991**, *91*, 1427.

(4) Dec, S. F.; Wind, R. A.; Maciel, G. E. *Macromolecules* **1987**, *20*, 2754.

(5) Miller, J. M. *Prog. NMR Spectrosc.* **1996**, *28*, 255.

(6) Isbester, P. K.; Kestner, T. A.; Munson, E. J. *Macromolecules* **1997**, *30*, 2800.

(7) Booth, J. P.; Hancock, G.; Perry, N. D.; Toogood, M. J. *J. Appl. Phys.* **1989**, *66*, 5251.

(8) Savage, C. R.; Timmons, R. B. *Chem. Mater.* **1991**, *3*, 575.

(9) Savage, C. R.; Timmons, R. B.; Lin, J. W. Spectroscopic Characterization of Films Obtained in Pulsed Radio-Frequency Plasma Discharges of Fluorocarbon Monomers. In *Advances in Chemistry Series*; American Chemical Society: Washington, DC, 1993; Vol. 236, p 745.

(10) Limb, S. J.; Edell, D. J.; Gleason, E. F.; Gleason, K. K. *Macromolecules*, submitted for publication.

(11) Wang, J.-H.; Chen, J.-J.; Timmons, R. B. *Chem. Mater.* **1996**, *8*, 2212.

(12) Kay, E.; Coburn, J.; Dilks, A. Plasma Chemistry of Fluorocarbons as Related to Plasma Etching and Plasma Polymerization. In *Topics in Current Chemistry*; Veprek, S., Venugopalan, M., Eds.; Springer-Verlag: Berlin, 1980; Vol. 94, p 1.

(13) Labelle, C. B.; Limb, S. J.; Gleason, K. K. *J. Appl. Phys.* **1997**, *82*, 1784.

(14) Limb, S. J.; Edell, D. J.; Gleason, E. F.; Gleason, K. K. *Chem. Mater.*, submitted for publication.

(15) Dixon, W. T. *J. Chem. Phys.* **1982**, *77*, 1800.

(16) Katoh, E.; Hiromi, S.; Kita, Y.; Ando, I. *J. Mol. Struct.* **1995**, *355*, 21.

(17) Tonelli, C.; Tortelli, V. *J. Fluorine Chem.* **1994**, *67*, 125.

(18) Emsley, J. W.; Phillips, L. *Prog. NMR Spectrosc.* **1971**, *7*, 1.

(19) Tortelli, V.; Tonelli, C.; Corvaja, C. *J. Fluorine Chem.* **1993**, *60*, 165.

(20) English, A. D.; Garza, O. T. *Macromolecules* **1979**, *12*, 351.

(21) Reimer, J. A.; Murphy, P. D.; Gerstein, B. C.; Knights, J. C. *J. Chem. Phys.* **1981**, *74*, 1501.

(22) Kessemeier, H.; Norberg, R. E. *Phys. Rev.* **1967**, *155*, 321.

(23) Knickelbein, M. B.; Webb, D. A.; Grant, E. R. *Mater. Res. Soc. Symp. Proc.* **1985**, *38*, 23.

(24) d'Agostino, R.; Cramarossa, F.; Illuzi, F. *J. Appl. Phys.* **1987**, *61*, 2754.

(25) Kirmse, K. H. R.; Wendt, A. E.; Disch, S. B.; Wu, J. Z.; Abraham, I. C.; Meyer, J. A.; Breun, R. A.; Woods, R. C. *J. Vac. Sci. Technol. B* **1996**, *14*, 710.

(26) Limb, S. J. Ph.D. Thesis, Massachusetts Institute of Technology, Cambridge, MA, 1997.

(27) Lewis, R. F.; Naylor, A. *J. Am. Chem. Soc.* **1947**, *69*, 1968.

(28) Bryant, W. M. D. *J. Polym. Sci.* **1962**, *56*, 277.

(29) Stoffels, W. W.; Stoffels, E.; Tachibana, K. *J. Vac. Sci. Technol. A* **1997**, *16*, 87.

(30) Fisher, W. K.; Corelli, J. C. *J. Polym. Sci., Polym. Chem. Ed.* **1981**, *19*, 2465.

(31) Theil, J. A.; Mertz, F.; Yairi, M.; Seaward, K.; Ray, G.; Kooi, G. *Mater. Res. Soc. Symp. Proc.*, in press.

(32) Creasy, W. R.; Zimmerman, J. A.; Jacob, W.; Kay, E. *J. Appl. Phys.* **1992**, *72*, 2462.

(33) Tutiya, M. Polytetrafluoroethylene (Effect of γ-Irradiation). In *Polymeric Materials Encyclopedia*; Salamone, J. C., Ed.; CRC Press: Boca Raton, FL, 1996; Vol. 9, p 6891.

(34) Wall, L. A. Thermal Decomposition of Fluoropolymers. In *Fluoropolymers*; Wall, L. A., Ed.; John Wiley & Sons: New York, 1972; p 381.

(35) Endo, K.; Tatsumi, T. *Appl. Phys. Lett.* **1996**, *68*, 2864.